Journal of
Materials Chemistry C

ROYAL SOCIETY
OF CHEMISTRY

PAPER

View Article Online
View Journal

Cite this: DOI: 10.1039/d5tc02304a

A multi-resonance TADF non-conjugated copolymer with near-unity photoluminescence quantum yield for efficient solution-processed OLEDs†

Rundong Tian, Zhi Yang, Zihan Wang, Jinxin Dong, Weihao Li, Guangfu Li* and Hui Xu *

Received 13th June 2025,
Accepted 3rd July 2025

DOI: 10.1039/d5tc02304a

rsc.li/materials-c

Multi-resonance thermally activated delayed fluorescence (MR-TADF) emitters have emerged as promising candidates for high-resolution OLEDs due to their near-unity exciton utilization efficiency and narrow-band emission. Highly efficient solution-processed OLEDs based on MR-TADF emitters are highly desired due to their combined advantages of cost-effective fabrication, compatibility with large-area flexible substrates, and potential to simultaneously achieve high color purity and superior device efficiency. Herein, we designed and synthesized a series of novel MR-TADF non-conjugated copolymers **PBN$_x$DPOT$_y$** by integrating MR-TADF moieties (DBNCz) and phosphine oxide moieties (DPOT) into non-conjugated polystyrene skeletons. This architecture synergistically combines narrow-band emission, through-space charge transfer (TSCT) with steric hindrance effects to achieve narrow emission (FWHM = 28–53 nm) with a record-high photoluminescence quantum yield (PLQY = 99.6%). Solution-processed OLEDs employing a **PBN3DPOT97** emitter demonstrate exceptional performance with an FWHM of 39 nm, EQE of 12.7%, and CIE coordinates of (0.16, 0.40). Theoretical calculation results show that the narrow-band emission in the copolymers **PBN$_x$DPOT$_y$** can be attributed to the MR-TADF moieties (DBNCz). Furthermore, spatial HOMO–LUMO distributions facilitates enhanced TSCT, resulting in superior device performance. This work establishes a new molecular design strategy for developing highly efficient MR-TADF non-conjugated copolymers for solution-processed OLEDs.

Introduction

Multi-resonance thermally activated delayed fluorescence (MR-TADF) emitters, distinguished by near-unity exciton utilization efficiency and exceptional spectral purity, have emerged as leading candidates for high-resolution organic light-emitting diodes (OLEDs).[1–9] Recent studies have primarily concentrated on heteroatom-embedded polycyclic aromatic structures, among which boron–nitrogen (B–N) co-doped systems constitute the most widely investigated structural motif.[8,10–16] In these systems, owing to the opposite electronic effect of B and N atoms in a polycyclic skeleton, the highest occupied molecular orbitals (HOMOs) and lowest unoccupied molecular orbitals (LUMOs) can be localized alternately on the adjacent atoms, resulting in a small singlet–triplet state energy gap ($\Delta E_{\mathrm{S-T}}$) with efficient TADF emission.[17–23] Furthermore, the structural rigidity of the emitter substantially suppresses vibrational relaxation of excited states, thereby giving rise to narrow-band emission with remarkably reduced full widths at half maximum (FWHM) ($<$ 50 nm).[24–32] Therefore, MR-TADF materials are expected to be an effective solution for developing organic light-emitting diodes (OLEDs) that simultaneously achieve high color purity and superior efficiency.[33–38]

Currently, most BN-embedded multi-resonance systems are based on small organic molecules, which often suffer from inferior solubilities, leading to the fabrication of corresponding OLED devices primarily through vacuum deposition techniques. In contrast, solution-processed OLEDs emerge as a compelling alternative owing to their cost-efficient production and inherent suitability for large-area flexible fabrication. TADF polymers serve as superior alternatives due to their excellent solubility in common organic solvents and ability to produce uniform films, which are critical for achieving highly efficient electroluminescence. Conjugated TADF polymers utilize rigidly planar architectures to facilitate through-bond charge transfer (TBCT), enabled by the constrained spatial alignment of donor

---

Key Laboratory of Functional Inorganic Material Chemistry, Ministry of Education, School of Chemistry and Material Science, Heilongjiang University, Harbin 150080, China. E-mail: gfli@hlju.edu.cn, hxu@hlju.edu.cn

† Electronic supplementary information (ESI) available: Experimental details, Gaussian simulation results, and photophysical and electroluminescence properties. See DOI: **https://doi.org/10.1039/d5tc02304a**

(D) and acceptor (A) moieties.[39] However, extended π-conjugation in these systems enhances donor–acceptor electronic coupling, resulting in significant frontier orbital overlap between HOMOs and LUMOs. This overlap elevates the singlet–triplet energy gap ($\Delta E_{\text{S-T}}$), thereby suppressing reverse intersystem crossing (RISC).[40] Moreover, competitive exciton dynamics between the conjugated skeleton and TADF-active segments frequently constrain electroluminescence efficiency. Therefore, to date, only a limited number of conjugated TADF polymers have achieved high external quantum efficiencies (EQEs) surpassing 23%.[41,42] In contrast, non-conjugated TADF polymers utilize flexible aliphatic skeletons, which confer three key advantages: (1) improved solution processability, (2) suppressed aggregation-caused quenching, and (3) the tunable design of peripheral substituent groups. In non-conjugated TADF polymer system, TADF can be realized by the intra- and inter-chains through-space charge transfer (TSCT) strategy. This architecture decouples electronic interactions, simultaneously reducing HOMO–LUMO overlap and minimizing $\Delta E_{\text{S-T}}$, which is essential for efficient RISC.[43,44] However, excessive through-TSCT can exacerbate non-radiative decay, particularly at high concentrations.[45] Therefore, attaining a synergistic equilibrium between these competing pathways to optimize exciton utilization remains a significant challenge. Furthermore, non-conjugated copolymer devices usually suffer from poor charge carrier transport, which severely restricts the development and practical application of non-conjugated copolymer-based OLEDs. Fortunately, introducing electron-withdrawing groups (*e.g.*, phosphine oxide (PO)) can enhance intramolecular charge transfer without compromising spatial separation, which facilitates charge carrier transport in devices, thereby enhancing device efficiency.[46]

Herein, we propose an innovative design strategy integrating non-conjugated architectures with MR-TADF moieties and electron-withdrawing phosphine oxide moieties, enabling high performance OLEDs based on non-conjugated polymer emitters. MR-TADF moieties ensure narrowband emission with high PLQYs, whereas phosphine oxide moieties serve as electron acceptors, facilitating both intra- and inter-chain TSCT to promote charge carrier transport and recombination in devices. Moreover, the substantial steric hindrance effect arising from both MR-TADF and phosphine oxide moieties enables further suppressing non-radiative transitions and balancing charge transport and recombination dynamics by precisely controlling the doping ratios. Inspired by this strategy, in this work, four new non-conjugated copolymers **PBN$_x$DPOT$_y$** featuring a polystyrene skeleton, with branched-chain modified MR-TADF moieties (DBNCz) and triazine-phosphine oxide moieties (DPOT), were designed and synthesized. All four polymers showed intense photoluminescence with FWHM in the range of 28–53 nm in the pristine film state. The corresponding PLQY of **PBN$_{10}$DPOT$_{90}$** is as high as 99.6%. To our best knowledge, this represents the highest reported PLQY among all those reported for MR-TADF polymers to date.[40,47,48]

Owing to their exciting photoluminescence properties, these four polymers were employed as emitters in solution-processed OLEDs. Among them, **PBN$_3$DPOT$_{97}$** displayed the best electroluminescence performance with a FWHM of 39 nm, EQE_{max} of 12.7%, the maximum brightness of up to 1024.6 cd m^{-2} and CIE coordinates of (0.16, 0.40) at a doping concentration of 10% using 10-(4-(4-(9*H*-carbazole-9-yl)phenylsulfonyl)phenyl)-9,9-dimethyl-9,10-dihydroacridine (CzAcSF) as the host material. Natural transition orbital (NTO) analysis reveals that the narrow-band emission stems from the MR-TADF core (DBNCz), leading to highly efficient MR-TADF emission. Furthermore, the spatial distributions of the HOMOs and LUMOs indicate a pronounced TSCT process in the ground state (S_0), promoting efficient carrier transport in devices and thus improving device performance. In summary, we integrate steric hindrance effects, MR-TADF, and TSCT to achieve highly efficient MR-TADF emission in non-conjugated polymers with superior device performance.

Results and discussion

Molecular design and structures

As shown in Fig. 1, polystyrene is selected as a non-conjugated skeleton, whereas the MR-TADF core (DBNCz) and electron acceptor (DPOT) are introduced into the skeleton in different molar ratios of 1/99, 3/97, 5/95 and 10/90, respectively. Four new non-conjugated MR-TADF copolymers **PBN$_x$DPOT$_y$** were synthesized *via* conventional free radical polymerization using azobisisobutyronitrile (AIBN) as the initiator. Its chemical structure and DBNCz/DPOT molar ratios were verified by nuclear magnetic resonance (NMR) spectroscopy (Fig. S1–S4, ESI†). These four copolymers exhibit a number-average molecular weight (M_n) of 18–21 kDa, corresponding to 39–45 repeat units (Table S2, ESI†), with a narrow polydispersity index (PDI = 1.42–1.51). The high molecular weight endows the copolymers with a thermal decomposition temperature exceeding 360 °C (Fig. S5, ESI†). In addition, all four copolymers demonstrate excellent solubility in common organic solvents (*e.g.*, chlorobenzene), rendering them suitable for solution-processed device fabrication.

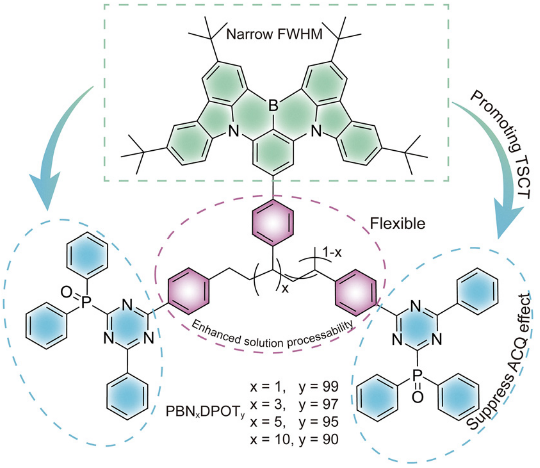

Fig. 1 The chemical structures of copolymers **PBN$_x$DPOT$_y$** with polystyrene as the non-conjugated skeleton, DBNCz as the MR-TADF core and DPOT as the electron acceptor, respectively.

Photophysical properties

The UV-vis absorption and excitation spectra of the copolymers **PBN$_x$DPOT$_y$** in the pristine film state are shown in Fig. 2a. All four copolymers exhibit nearly the same characteristic with two main absorption peaks. The strong absorption peak in the range of 230–250 nm refers to local π–π* transitions arising from DBNCz and DPOT units, whereas relative weak absorption peak of 288 nm can be attributed to the charge transfer excited state originating from the intra- and inter-chain interactions between DBNCz and DPOT units. The excitation spectra of four copolymers showed similar characteristics with peaks in the range of 300–302 nm. The photoluminescence (PL) spectra of all four copolymers in the pristine film state are shown in Fig. 2b. The steady state emission spectra show a narrow-band emission feature with FWHM of 28, 34, 42, 53 nm, respectively, with the maximum emission wavelength of 489 nm, 493 nm, 495 nm and 497 nm, respectively. This result indicates that the red-shifted emission and broadening FWHM can be induced by the increment of molar ratio of the MR-TADF group (DBNCz), which might be attributed to the enhanced D–A interaction between DBNCz and DPOT. Furthermore, the FWHM can be reasonable regulated by decreasing the ratio of the MR-TADF (DBNCz) unit. The basically consistent (prompt fluorescence) PF, (delayed fluorescence) DF and (phosphorescence) PH spectra indicate that the energy level between the singlet state and the triplet state is extremely small for all four copolymers, which is beneficial for accelerating the RISC process and restricting the non-radiative transition process simultaneously. It is worth noting that all four copolymers show highly efficient emission with the photoluminescence quantum yield (PLQY) exceeding 89% (Table S3, ESI†). The PLQY increases with an increase in the molar ratio of the MR-TADF (DBNCz) unit. Particularly, **PBN$_{10}$DPOT$_{90}$** showed an amazing near-unity PLQY of 99.6%. This result indicates that the emission efficiency can be reasonably adjusted by controlling the doping ratio of DBNCz/DPOT units. Fig. 2c shows the comparison of time decays of four copolymers **PBN$_x$DPOT$_y$** at room temperature. All four copolymers exhibit bi-exponential delayed fluorescence (DF) decay curves with lifetime in the range of 9.31–9.72 μs. Notably, the nanosecond-scale lifetime component increases with increasing DPOT units concentration (Fig. 2c, inset), further confirming their TADF characteristics. Furthermore, time-resolved emission spectra (TRES) of **PBN$_3$DPOT$_{97}$** reveal almost unchanged emission wavelength and life decays during radiation at 50–300 K, indicating an improvement in the thermal equilibrium of RISC and triplet quenching (Fig. 2d).[49] Therefore, all these results demonstrate that the MR-TADF emission of the copolymers originates from the MR-TADF core (DBNCz). Furthermore, the substantial steric hindrance effect introduced by both DBNCz and DPOT units promote TSCT through both intra- and

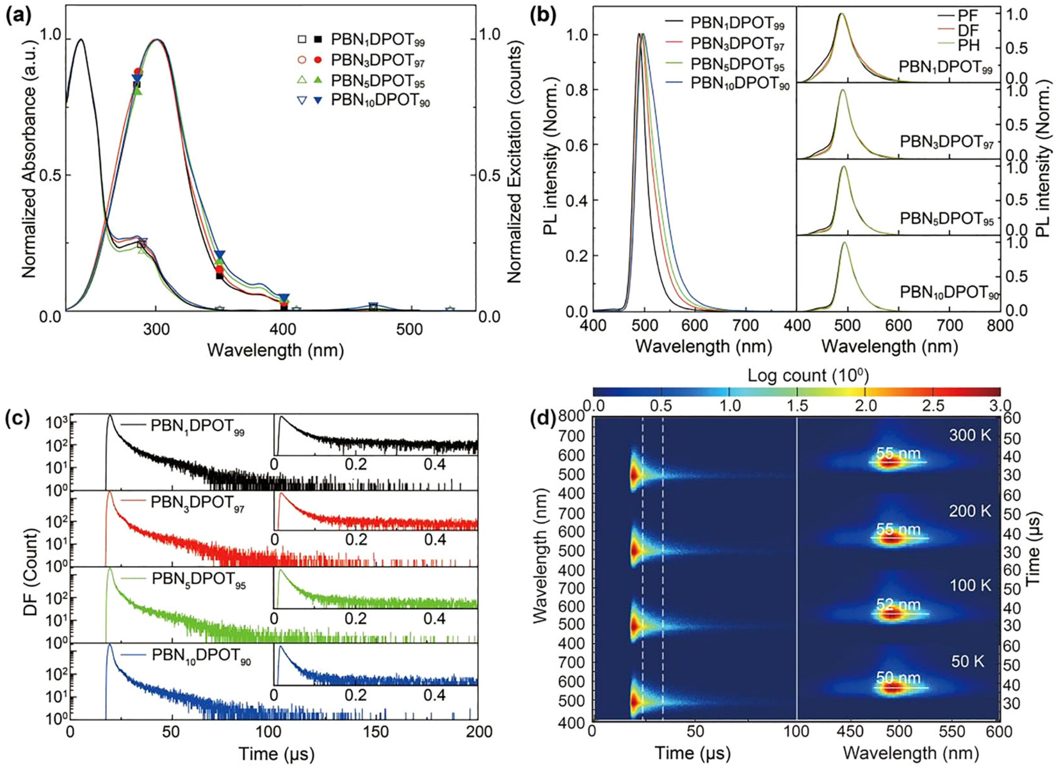

Fig. 2 Photophysical properties of **PBN$_x$DPOT$_y$** copolymers. (a) The normalized UV absorption (hollow symbol) and excitation (solid symbol) spectra of the copolymers **PBN$_x$DPOT$_y$** in the pristine film state; (b) the steady PL, PF, DF and PH spectra of the copolymers **PBN$_x$DPOT$_y$** in the pristine film state; (c) the comparison of time decays of four copolymers **PBN$_x$DPOT$_y$** in the pristine film state at room temperature (inset: PF decay with nanosecond lifetime); (d) time-related emission spectra (TRES) of **PBN$_3$DPOT$_{97}$** in the pristine film state, at room temperature and variable temperatures at 50, 100, 200 and 300 K, respectively.

inter-chain interactions, thereby not only reducing singlet and triplet state energy gaps to accelerate the RISC process, but also effectively suppressing non-radiative transition pathways, as evidenced by the enhanced photoluminescence quantum yield.

Theoretical calculations

The oligomers containing two DPOT units and one DBNCz multi-resonance unit were simulated to evaluate the electronic properties of the corresponding copolymers. As shown in Fig. 3a and Fig. S7 (ESI†), HOMOs (including HOMO, HOMO−1 and HOMO−2) and LUMOs (including LUMO, LUMO+1 and LUMO+2) are located on DBNCz and DPOT, respectively, which indicates the obvious TSCT process happening between DBNCz and DPOT in the ground state. The DPOT units significantly enhance inter-chain charge transportation due to the strong electron-withdrawing ability of DPOT, which is consistent with the experimental results of cyclic voltammetry analysis (Fig. S6, ESI†). Natural transition orbit (NTO) analysis was conducted to identify the excited state characteristics of oligomers under the excitation of $S_0 \rightarrow S_1$ and $S_0 \rightarrow T_1$ (Fig. 3b). The ''holes'' and ''electrons'' of the S_1 and T_1 states of the **PBN$_x$DPOT$_y$** oligomer significantly overlap on the DBNCz group, corresponding to the excited state characteristic of MR-TADF, which is consistent with the experimental PL characteristic with narrow-band emission. The theoretically calculated $\Delta E_{\mathrm{S-T}}$ is 0.38 eV, which is beneficial for achieving effective RISC, and further improving the TADF performance.

Electroluminescence properties

To evaluate the EL performance of the **PBN$_x$DPOT$_y$** emitters, solution-processed OLEDs were fabricated with device configuration of ITO/PEDOT:PSS (60 nm)/PVK (30 nm)/CzAcSF:*x*% **PBN$_x$DPOT$_y$** emitters (30 nm)/TmPyPB (35 nm)/LiF (1 nm)/Al (100 nm), where poly(3,4-ethylenedioxythiophene)/poly(styrenesulfonate) PEDOT:PSS and LiF were used as hole- and electron-injection layers, polyethylene carbazole (PVK) and 1,3,5-tri[(3-pyridyl)-phen-3-yl]benzene (TmPyPB) were used as hole- and electron-transporting layers, and 10-(4-(4-(9*H*-carbazole-9-yl)phenylsulfonyl)phenyl)-9,9-dimethyl-9,10-dihydroacridine (CzAcSF) was employed as the host material. The doping concentration of guest emitters was 1, 5, 10, and 15%, respectively.

The device configuration and energy level diagram are given in Fig. 4a. The steady EL spectra for all devices are shown in Fig. S9 (ESI†), and detailed EL performance for all devices are summarized in Table S5 (ESI†). It can be seen that the FWHM of the EL spectra ranges from 36 to 73 nm. Through systematic screening and comparison of the devices based on different doping ratios between **PBN$_x$DPOT$_y$** and CzAcSF, the device based on **PBN$_3$DPOT$_{97}$** demonstrates optimal overall performance, enabling it to be a representative device to discuss. As shown in Fig. 4b, all four devices show narrow-band electroluminescence feature with intense green emission with peaks of ∼490 nm. The narrowest FWHM of 36 nm was achieved at the guest doping concentration of 1%. The corresponding Commission Internationale de L'Eclairage coordinates (CIE) are (0.16, 0.40). These results indicate that the narrow-band electroluminescence resulting from the guest emitter

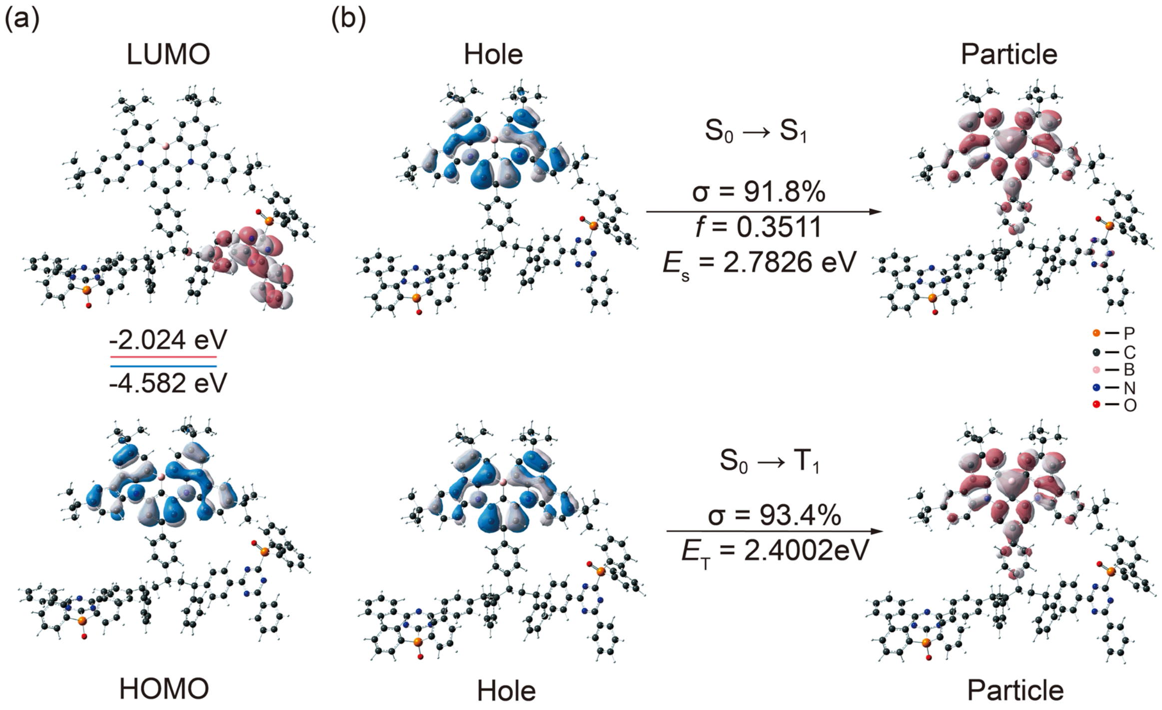

Fig. 3 (a) The HOMO and LUMO distributions of **PBN$_x$DPOT$_y$** oligomers, and corresponding energy levels; (b) natural transition orbitals of **PBN$_x$DPOT$_y$** oligomers under the excitation of $S_0 \rightarrow S_1$ and $S_0 \rightarrow T_1$.

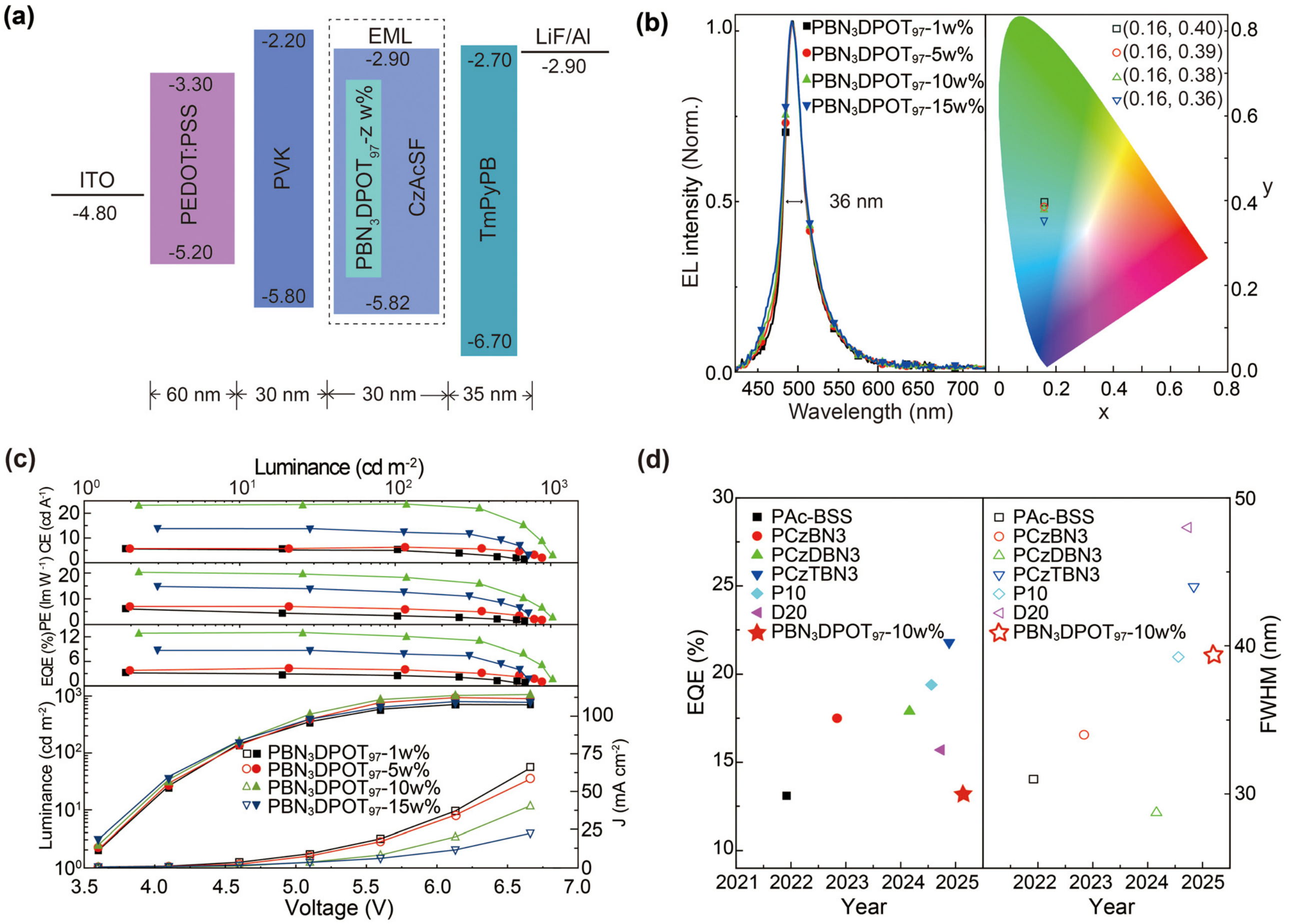

Fig. 4 (a) Device configuration and the related energy levels; (b) the normalized EL spectra and the corresponding CIE coordinates of the devices based on the $\mathbf{PBN_3DPOT_{97}}$ emitter with doping concentrations of 1, 5, 10 and 15%, respectively; (c) current density (hollow symbols)–voltage–luminance (solid symbols) curves and efficiency–luminance curves of devices based on $\mathbf{PBN_3DPOT_{97}}$ with doping concentrations of 1, 5, 10, and 15%, respectively; (d) summary of external quantum efficiencies (EQEs) and FWHM for representative devices based on MR-TADF polymers since 2021.

$\mathbf{PBN_xDPOT_y}$ can be realized, which is consistent with photoluminescence properties.

The *J*–*V*–*L* characteristics and efficiencies *versus* luminance curves of these devices are depicted in Fig. 4c, and the key EL data are summarized in Table 1 and Table S5 (ESI†). All four devices display low driving voltages below 5.5 V at luminance of 10 cd m^{-2} and 100 cd m^{-2}. The device with a doping concentration of 10% achieves a maximum luminance over 1024.6 cd m^{-2} when the applied voltage is 6.7 V, which is comparable to that of state-of-the-art non-conjugated MR-TADF polymer based devices and meets the requirements for practical display applications.[50] The best device efficiency was measured at a concentration of 10% with maximum current efficiency (CE, η_{CE}), power efficiency (PE, η_{PE}), and external quantum efficiency (EQE) of 23.9 cd A^{-1}, 20.7 lm W^{-1} and 12.7%, respectively. It is worth noting that the efficiency roll-off is also well suppressed. When the luminance was up to 400 cd m^{-2}, the EQE still remains above 10.6%, and the efficiency roll-off was only 16.5%. The low efficiency roll-off can be attributed to the fast RISC process that is induced by the effectively

Table 1 EL performance of the $\mathbf{PBN_3DPOT_{97}}$ emitter

Polymer	*z* (w%)	V^a (V)	$L_{max}{}^b$ (cd m^{-2})	η^c η_{CE} (cd A^{-1})	η_{PE} (lm W^{-1})	η_{EQE} (%)	FWHM (nm)	λ_{EL} (nm)/CIE (*x*, *y*)^d
$\mathbf{PBN_3DPOT_{97}}$-zw%	1	3.7, 4.5, 5.5	667.2	5.1, 4.0, 2.2	5.8, 5.1, 2.8	3.1, 3.0, 2.7	36	490/(0.16, 0.40)
	5	3.9, 4.5, 5.2	883.9	6.9, 6.3, 4.2	7.2, 7.0, 5.8	4.2, 4.1, 4.0	37	490/(0.16, 0.39)
	10	3.8, 4.4, 5.2	1024.6	23.9, 23.4, 16.9	20.7, 19.8, 17.6	12.7, 12.2, 11.9	39	491/(0.16, 0.38)
	15	3.7, 4.4, 5.4	703.0	14.2, 11.7, 8.4	15.2, 14.1, 12.3	8.8, 8.7, 7.5	41	491/(0.16, 0.36)

[a] At 10, 100 and 500 cd m^{-2}. [b] Maximum brightness. [c] EL efficiencies at the maximum and 10 and 100 cd m^{-2}, respectively. [d] Emission peaks and CIE color coordinates at 100 cd m^{-2}.

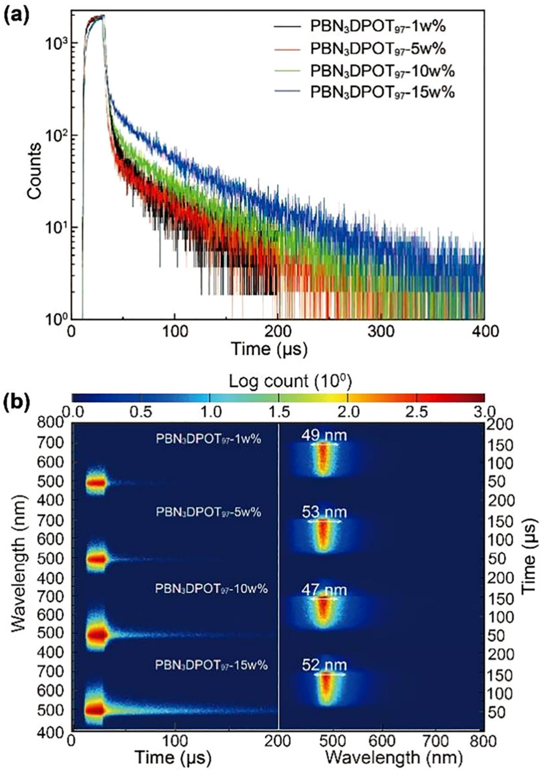

Fig. 5 (a) EL decay of **PBN_3DPOT_{97}** at different doping concentrations; (b) EL TREES and sliced TREES contours at 0–20 μs of **PBN_3DPOT_{97}**-zw%.

intra- and inter chain TSCT between DBNCz and DPOT.[51,52] Furthermore, the induction of the DPOT unit also effectively facilitates carrier flux balance in the EML, which is conducive to promoting the exciton utilization and further improving the device efficiency. Notably, the device based on the **PBN_3DPOT_{97}** emitter shows a maximum η_{EQE} of 12.7% with a FWHM of 39 nm, representing one of the best performances among the MR-TADF polymer devices with FWHM below 40 nm (Fig. 4d and Table S6, ESI†).

To further investigate the EL mechanism of the devices, the exciton kinetics using time-resolved EL spectroscopy was further studied. As shown in Fig. 5a and b, the lifetimes increase with the increment of doping concentration of guest emitters **PBN_3DPOT_{97}**, which is accompanied with the broadening of the EL spectra. The markedly longer EL decay of high doping concentration reveals more stable exciton trapping in interchain CT states. As shown in Table S5 (ESI†), the other three devices exhibit similar FWHM broadening trends with increasing doping concentration of **PBN_xDPOT_y**, reflecting the consistent result of formation of more inter-chain CT excitons. Furthermore, FWHM broadening trends are also presented by increasing the molar ratio of DPOT from **$PBN_{10}DPOT_{90}$** to **PBN_1DPOT_{99}**, which can be assigned to the formation of more inter-chain CT excitons by increasing the molar ratio of bulky conjugated electron-accepting group DPOT.

Conclusions

In summary, we have successfully designed and synthesized four new MR-TADF non-conjugated copolymer emitters by integrating MR-TADF moieties (DBNCz) and phosphine oxide moieties (DPOT) into polystyrene-based architectures. The MR-TADF core ensured efficient narrow-band emission (FWHM 28–53 nm) with record-high PLQYs up to 99.6%. The introduction of bulky conjugated phosphine oxide moieties DPOT, also contribute to the high PLQYs by suppressing the non-radiative decay. Furthermore, DPOT moieties enable effective TSCT for balanced carrier transport to further improve the electroluminescence performance. The resulting solution-processed OLEDs achieved maximum brightness, current efficiency (CE), power efficiency (PE), and external quantum efficiency (EQE) of 1024.6 cd m^{-2}, 23.9 cd A^{-1}, 20.7 lm W^{-1} and 12.7%, respectively. The FWHM in EL spectra ranged from 36 to 73 nm, exhibiting an increasing trend with an increase in the doping concentration of the guest emitters **PBN_xDPOT_y**. Moreover, the efficiency roll-off was also well suppressed. When the luminance was up to 400 cd m^{-2}, the EQE still remained above 10.6%, and the efficiency roll-off was only 16.5%. This represents a significant advancement in non-conjugated MR-TADF polymer emitters. Therefore, this study provides a promising strategy for designing efficient MR-TADF non-conjugated copolymer emitters, which show great potential in the development of high-performance solution-processed OLEDs with narrow-band emission characteristics.

Author contributions

H. X. conceived, designed, and supervised the project. R. T. synthesized materials and prepared the devices, and performed photophysical investigation with contributions from J. D., Z. W., W. L., and Z. Y. measured electroluminescence properties. R. T. and G. L. and H. X. co-wrote the manuscript. All authors participated in the discussion and analysis of the manuscript.

Conflicts of interest

There are no conflicts to declare.

Data availability

The data that support the findings of this study are available from authors but restrictions apply to the availability of these data, which were used under license for the current study, and so are not publicly available.

Acknowledgements

The financial support from the National Natural Science Foundation of China (No. 22375057, W2412073, 52273173, 22325502, 92461304, 22305073, and 52203213) is highly acknowledged.

References

1 S. M. Suresh, D. Hall, D. Beljonne, Y. Olivier and E. Zysman-Colman, *Adv. Funct. Mater.*, 2020, **30**, 1908677.

2 K. R. Naveen, H. I. Yang and J. H. Kwon, *Commun. Chem.*, 2022, **5**, 149.

3 R. Braveenth, K. Raagulan, Y.-J. Kim and B.-M. Kim, *Adv. Mater.*, 2023, **4**, 374–388.

4 H. Jiang, J. Jin and W.-Y. Wong, *Adv. Funct. Mater.*, 2023, **33**, 2306880.

5 Y. Xu, Q. Wang, X. Cai, C. Li, S. Jiang and Y. Wang, *Angew. Chem., Int. Ed.*, 2023, **62**, e202312451.

6 X. Zhu, Y. Zhang, J. Miao, J. Liu and L. Wang, *Angew. Chem., Int. Ed.*, 2024, **63**, e202411023.

7 T. Hua, J. Miao, H. Xia, Z. Huang, X. Cao, N. Li and C. Yang, *Adv. Funct. Mater.*, 2022, **32**, 2201032.

8 G. Chen, J. Miao, X. Huang, Z. Zhang, Z. Xue, M. Huang, N. Li, X. Cao, Y. Zou and C. Yang, *Light: Sci. Appl.*, 2025, **14**, 81.

9 J. Zhang, J. Sun, Y. Ma, C. Han, D. Ding, Y. Wei and H. Xu, *Adv. Funct. Mater.*, 2022, **32**, 2209163.

10 K. Zhang, X. Wang, M. Wang, S. Wang and L. Wang, *Angew. Chem., Int. Ed.*, 2025, **64**, e202423812.

11 X. Lv, J. Miao, M. Liu, Q. Peng, C. Zhong, Y. Hu, X. Cao, H. Wu, Y. Yang, C. Zhou, J. Ma, Y. Zou and C. Yang, *Angew. Chem., Int. Ed.*, 2022, **61**, e202201588.

12 Y. Guo, W. Xie, Z. Ye, K. Xu, Z. Zhang, Z. Xiao, J. Miao, Y. Zou, C. Zhong, X. Yin, C. Yang and X. Cao, *Angew. Chem., Int. Ed.*, 2025, **64**, e202503320.

13 K. Xu, N. Li, Z. Ye, Y. Guo, Y. Wu, C. Gui, X. Yin, J. Miao, X. Cao and C. Yang, *Chem. Sci.*, 2024, **15**, 18076–18084.

14 T. Wang, X. Yin, X. Cao and C. Yang, *Angew. Chem., Int. Ed.*, 2023, **62**, e202301988.

15 Y.-J. Yu, Z.-Q. Feng, X.-Y. Meng, L. Chen, F.-M. Liu, S.-Y. Yang, D.-Y. Zhou, L.-S. Liao and Z.-Q. Jiang, *Angew. Chem., Int. Ed.*, 2023, **62**, e202310047.

16 B. Cui, J. Zhou, C. Duan and H. Xu, *Adv. Opt. Mater.*, 2025, **13**, 2403295.

17 Z. Jiang, Q. Chen, C. Shi, J. Su, F. Li, K. Ye, Z. Zhao, Q. Li, A. Yuan and G. Xie, *Dyes Pigm.*, 2025, **236**, 112681.

18 C. Wang, N. Hu, Z. Chen, Y. Chen, P. Chang, C. Han, X. Cao and H. Xu, *Chem. Eng. J.*, 2024, **488**, 150785.

19 W.-C. Guo, W.-L. Zhao, K.-K. Tan, M. Li and C.-F. Chen, *Angew. Chem., Int. Ed.*, 2024, **63**, e202401835.

20 S. Chen, Y. Wang, J. Lin, R. Tian, S. Li, Y. Man, S. Chen, J. Zhang, C. Duan, C. Han and H. Xu, *Chem. Eng. J.*, 2024, **489**, 151517.

21 Y. Yang, N. Li, J. Miao, X. Cao, A. Ying, K. Pan, X. Lv, F. Ni, Z. Huang, S. Gong and C. Yang, *Angew. Chem., Int. Ed.*, 2022, **61**, e202202227.

22 J. Bian, S. Chen, L. Qiu, R. Tian, Y. Man, Y. Wang, S. Chen, J. Zhang, C. Duan, C. Han and H. Xu, *Adv. Mater.*, 2022, **34**, 2110547.

23 Y. Xu, Q. Wang, X. Cai, C. Li and Y. Wang, *Adv. Mater.*, 2021, **33**, 2100652.

24 J. Bian, S. Chen, L. Qiu, N. Zhang, J. Zhang, C. Duan, C. Han and H. Xu, *Research*, 2022, **2022**, 9838120.

25 Q. Wang, Y. Xu, T. Huang, Y. Qu, J. Xue, B. Liang and Y. Wang, *Angew. Chem., Int. Ed.*, 2023, **62**, e202301930.

26 Z. Wang, Y. Man, C. Zhang, Y. Pang, Y. Wei, J. Zhang, C. Shuo, C. Duan, C. Han, C. Cao, X. Shui and H. Xu, *Adv. Opt. Mater.*, 2024, **12**, 2302046.

27 T. Hatakeyama, K. Shiren, K. Nakajima, S. Nomura, S. Nakatsuka, K. Kinoshita, J. Ni, Y. Ono and T. Ikuta, *Adv. Mater.*, 2016, **28**, 2777–2781.

28 H. Lim, S.-J. Woo, Y. H. Ha, Y.-H. Kim and J.-J. Kim, *Adv. Mater.*, 2022, **34**, 2100161.

29 J. Park, K. J. Kim, J. Lim, T. Kim and J. Y. Lee, *Adv. Mater.*, 2022, **34**, 2108581.

30 J. Liu, Y. Zhu, T. Tsuboi, C. Deng, W. Lou, D. Wang, T. Liu and Q. Zhang, *Nat. Commun.*, 2022, **13**, 4876.

31 Y. Kondo, K. Yoshiura, S. Kitera, H. Nishi, S. Oda, H. Gotoh, Y. Sasada, M. Yanai and T. Hatakeyama, *Nat. Photonics*, 2019, **13**, 678–682.

32 Y. Sano, T. Shintani, M. Hayakawa, S. Oda, M. Kondo, T. Matsushita and T. Hatakeyama, *J. Am. Chem. Soc.*, 2023, **145**, 11504–11511.

33 M. Yang, I. S. Park and T. Yasuda, *J. Am. Chem. Soc.*, 2020, **142**, 19468–19472.

34 M. Yang, S. Shikita, H. Min, I. S. Park, H. Shibata, N. Amanokura and T. Yasuda, *Angew. Chem., Int. Ed.*, 2021, **60**, 23142–23147.

35 J.-K. Li, X.-Y. Chen, Y.-L. Guo, X.-C. Wang, A. C. H. Sue, X.-Y. Cao and X.-Y. Wang, *J. Am. Chem. Soc.*, 2021, **143**, 17958–17963.

36 B. Lei, Z. Huang, S. Li, J. Liu, Z. Bin and J. You, *Angew. Chem., Int. Ed.*, 2023, **62**, e202218405.

37 D. Li, M. Li, D. Liu, J. Yang, W. Li, Z. Yang, H. Yuan, S. Jiang, X. Peng, G.-X. Yang, W. Xie, W. Qiu, Y. Gan, K. Liu and S.-J. Su, *Adv. Opt. Mater.*, 2023, **11**, 2301084.

38 H.-J. Cheon, S.-J. Woo, S.-H. Baek, J.-H. Lee and Y.-H. Kim, *Adv. Mater.*, 2022, **34**, 2207416.

39 S. Shao, Z. Ma, J. Ding, L. Wang, X. Jing and F. Wang, *Adv. Mater.*, 2012, **24**, 2009–2013.

40 W. Luo, T. Wang, Z. Huang, H. Huang, N. Li and C. Yang, *Adv. Funct. Mater.*, 2024, **34**, 2310042.

41 Z. Zhao, Y. Liu, L. Hua, S. Yan and Z. Ren, *Adv. Funct. Mater.*, 2022, **32**, 2200018.

42 J. Rao, L. Yang, X. Li, L. Zhao, S. Wang, H. Tian, J. Ding and L. Wang, *Angew. Chem., Int. Ed.*, 2021, **60**, 9635–9641.

43 R. Wei, H.-Y. Chi, X. Li, D. Lu, Y. Wan, C.-W. Yang and Z. Lai, *Adv. Funct. Mater.*, 2020, **30**, 1907089.

44 S. Shao, J. Hu, X. Wang, L. Wang, X. Jing and F. Wang, *J. Am. Chem. Soc.*, 2017, **139**, 17739–17742.

45 F. Milos, G. Tullii, F. Gobbo, F. Lodola, F. Galeotti, C. Verpelli, D. Mayer, V. Maybeck, A. Offenhäusser and M. R. Antognazza, *ACS Appl. Mater. Interfaces*, 2021, **13**, 23438–23451.

46 J. Dong, Y. Xu, S. Wang, J. Miao, N. Li, Z. Huang and C. Yang, *Chem. Commun.*, 2024, **60**, 6789–6792.

47 T. Wang, Z. Huang, H. Zhang, J. Miao and C. Yang, *Adv. Funct. Mater.*, 2024, **34**, 2408119.

48 T. Wang, Y. Zou, Z. Huang, N. Li, J. Miao and C. Yang, *Angew. Chem., Int. Ed.*, 2022, **61**, e202211172.

49 Y. Xin, Y. Zhu, R. Chi, C. Duan, P. Yan, C. Han and H. Xu, *Adv. Mater.*, 2023, **35**, 2304103.

50 F. Chen, L. Zhao, X. Wang, Q. Yang, W. Li, H. Tian, S. Shao, L. Wang, X. Jing and F. Wang, *Sci. China: Chem.*, 2021, **64**, 547–551.

51 C. Wu, W. Liu, K. Li, G. Cheng, J. Xiong, T. Teng, C.-M. Che and C. Yang, *Angew. Chem., Int. Ed.*, 2021, **60**, 3994–3998.

52 D. Li, J. Yang, J. Chen, X. Peng, W. Li, Z. Chen, W. Qiu, G.-X. Yang, Z. Yang, M. Li, S. Jiang, D. Liu, Y. Gan, K. Liu and S.-J. Su, *Mater. Chem. Front.*, 2023, **7**, 1128–1136.